THE ASTROPHYSICAL JOURNAL, 377:227–234, 1991 August 10

ULTRAVIOLET AND OPTICAL SPECTROSCOPY OF THE R AQUARII SYMMETRICAL JET

J. M. HOLLIS,[1] R. J. OLIVERSEN,[2] M. KAFATOS,[3] A. G. MICHALITSIANOS,[2] AND R. M. WAGNER[4]

Received 1990 December 5; accepted 1991 February 6

ABSTRACT

The first ultraviolet spectrum of the southwest (SW) component of the symmetrical jet in the R Aquarii binary system has been obtained in the range 1200–2000 Å with the *International Ultraviolet Explorer* (*IUE*). These results are compared to more encompassing spectra (1200–3200 Å) of the central H II region taken at the same time and also similar spectra of the northeast (NE) jet component obtained 6 months earlier. Moreover, optical spectra of both the NE and SW jet components in the range 3400–9800 Å were obtained within ~6 months and ~1 month, respectively, of the ultraviolet spectra. These highly complementary observations argue that excitation of the symmetrical jet may be due to shock excitation as the jet components overtake and impact the previously ionized material associated with the expanding inner nebulosity. We discuss the problems with this shock model as well as problems with competing photoionization models. We suggest that the jet components were ejected less than 90 years ago.

Subject headings: nebulae: H II regions — nebulae: individual (R Aquarii) — nebulae: structure — stars: individual (R Aquarii) — ultraviolet: spectra

1. INTRODUCTION

The R Aquarii symbiotic system (M7e+pec) has been studied extensively in recent years for stellar jet activity; the jet components are embedded in a 1′ inner nebula elongated north-south. This inner nebula is embedded in a 2′ outer nebula oriented east-west. At 250 pc (Whitelock 1987), R Aqr would be the nearest astrophysical jet source, and, hence, detailed investigations of its emission may provide important clues concerning astrophysical jet phenomena in general. A jet of material was originally detected in the optical, protruding ~6″ or ~1500 AU from the 387 day Mira variable (Wallerstein & Greenstein 1980; Herbig 1980) toward the northeast. Subsequent radio continuum observations showed that the optical and radio emission were cospatial and the presence of a weak counterjet was indicated (Hollis et al. 1985). An optical image by Mauron et al. (1985) also suggested that there may well be a southwest (SW) component in addition to the stronger northeast (NE) component.

Very Large Array (VLA) 6 cm continuum data acquired over the course of 5 years (Kafatos et al. 1989) demonstrated that the R Aqr jet was symmetrical, presenting bipolar morphology; these observations indicated that the emission extended ~2500 AU from the central object in both directions. By means of high-resolution spectroscopic observations of Hβ and [O III] at 4959 and 5007 Å, Hollis, Wagner, & Oliversen (1990) showed that the SW and NE jet components have an average recessional radial velocity of ~100 km s^{-1} relative to each other; bipolar [O III] emission was also discovered extending to distances of ~2750 AU on either side of the Mira variable.

There are indications that the jet is evolving on a time scale of years. For example, Kafatos, Michalitsianos, & Hollis (1986) presented ultraviolet evidence that the NE jet brightened in C IV $\lambda\lambda$1548, 1550 over the course of ~5.5 yr of *IUE* monitoring. Further, the NE jet's sudden appearance (around the late 1970s) and the SW jet's seemingly increasing flux at visible wavelengths (cf. Hollis et al. 1990; Solf & Ulrich 1985) suggest that the symmetrical jet components were brightening. Other observations which may indicate temporal changes of optical emission knots within the NE jet were noted by Paresce, Burrows, & Horne (1988) and Burgarella & Paresce (1991). Hence, we were motivated to probe the SW and NE jet components from ~1200 to ~9800 Å to determine the nature of the jet excitation.

2. OBSERVATIONS AND DATA REDUCTION

2.1. *Ultraviolet*

IUE observations of the SW jet and central H II region were obtained with the large (10″ × 20″) entrance aperture, using the low-resolution (LORES; $\Delta\lambda \sim 6$ Å) SWP 1200–1950 Å and LWP 1850–3200 Å cameras on 1989 December 28. The aperture was offset from the Mira variable (central H II region) ~13″ southwest of R Aqr. This offset was derived from [O III] λ5007 images (Hollis et al. 1990) with the aperture centered at the position of peak [O III] emission. The offset to the SW jet was sufficiently large that guiding on R Aqr itself was feasible, and any contributions from instrument-scattered ultraviolet emission from the central H II region was negligible in the resultant SW jet spectrum. The R Aqr position on the sky ensures that the spacecraft roll angle (~110° for these observations) will always result in the long axis of the aperture being nearly perpendicular to the jet axis; this precludes obtaining spatial and spectral information for both the NE and the SW jets in the same exposure.

Similarly, LORES large aperture SWP and LWP spectra of the NE jet were obtained on 1989 June 5 at a spacecraft roll angle of ~295°. The aperture was centered on the peak VLA 6 cm continuum position of the NE jet (Kafatos, Hollis, & Michalitsianos 1983). In these observations a faint guide star was used, since R Aqr itself was too close to the NE jet position.

[1] Space Data and Computing Division, NASA/Goddard Space Flight Center, Code 930, Greenbelt, MD 20771.
[2] Laboratory for Astronomy and Solar Physics, NASA/Goddard Space Flight Center, Code 684, Greenbelt, MD 20771.
[3] Department of Physics, George Mason University, Fairfax, VA 22030.
[4] Department of Astronomy, Ohio State University, Lowell Observatory, Mars Hill Road, 1400 West, Flagstaff, AZ 86001.

TABLE 1

JOURNAL OF *IUE* OBSERVATIONS

Feature	α(1950)	δ(1950)	Date	Exposure (minutes)	Camera and Sequence Number
NE jet	$23^h41^m14^s.5$	−15°33′35″	1989 Jun 5	200	SWP 36397
			1989 Jun 5	100	LWP 15662
H II region	23 41 14.3	−15 33 42.8	1989 Dec 28	40	SWP 37915
			1989 Dec 28	40	LWP 17024
SW jet	23 41 13.7	−15 33 52.4	1989 Dec 28	300	SWP 37914

Table 1 is a journal of all our *IUE* observations, and Table 2 contains the emission-line flux measurements which were calibrated using the extended source reduction method and the latest standard ITF extraction algorithms (Turnrose & Thompson 1984; Cassatella, Lloyd, & Gonzalez Riestra 1988). Figure 1 shows the SWP spectra obtained of the NE jet, the central H II region, and the SW jet. Comparison suggests that the NE and SW jets have similar density and excitation conditions. For example, in the SW jet, density-sensitive lines of Si III] at 1882 and 1892 Å were present. These Si III] lines were also present in the NE region (cf. Michalitsianos & Kafatos 1982; Kafatos et al. 1986). In the central H II region, the Si III] line at 1892 Å dominates over line emission at 1882 Å. The relative strengths of the two lines (Nussbaumer 1986) suggest that the NE and SW jet regions are considerably lower in density compared with the central H II region; that is, $n_e \sim 10^3$ to $\sim 10^4$ cm^{-3} in the jets and $n_e \sim 10^6$ cm^{-3} in the central H II region. Moreover, N V λλ1238, 1242 is relatively strong at both jet positions. This confirms previous observations of the NE jet (cf. Kafatos et al. 1986) which suggest higher excitation compared with the H II region, based upon N V as well as He II λ1640 emission. Higher excitation is also consistent with weak O I 1301–1304 Å emission in both the NE and SW jets.

The *IUE* spectra of the NE jet clearly show spatially extended structure in strong emission lines, particularly C IV λλ1548, 1550; C II] λ2328; and [O II] λ2470; which is consis-

TABLE 2

ULTRAVIOLET EMISSION-LINE FLUX MEASUREMENTS

Ion	Laboratory Wavelength (Å)	Flux (10^{-13} ergs cm^{-2} s^{-1})[a]		
		H II Region	NE Jet	SW Jet
N V	1238.8, 1242.8	4.2	6.3	1.2
Si II	1264.8	2.9	<0.5	0.2
O I	1302.1–1304.9	13.4	2.8	0.1
C II	1334.5, 1335.7	15.9	9.6	3.9
Si IV	1393.7	2.3	0.8	0.9
O IV]	1401.1–1407.4	2.3	3.8	0.4
N IV]	1483.3, 1486.5	5.9	2.4	0.5
C IV	1548.2, 1550.8	80.1	30.0	6.4
λ1594?		<1.0	<0.5	0.5
He II	1640.3	5.3	4.8	0.4
O III]	1660.8, 1666.2	26.7	11.4	1.9
N III]	1748.7–1753.9	18.6	7.3	2.0
Si II	1808.0, 1816.9	4.3	<0.5	0.2
Al III?	1854.7	1.4	<0.5	0.6
Si III]	1883.0, 1892.0	5.0	1.9	0.2
C III]	1906.7, 1909.7	>138.5	>49.4	>8.1
C II][b]	2328.1	76.9	46.6	...
[O II]	2470.3	27.1	15.4	...
Fe II	2631.2 (1)	2.1	4.4:	...
Fe II	2750.9	5.2	15.8	...
Mg II	2795.4, 2802.6	>36.7	>19.0	...
[Fe II]?	2835.7	5.4	10.8	...
Fe II?	3183.1	7.3	2.9	...

[a] Not corrected for extinction; 1 σ errors: strong, unsaturated lines (5%); weak, unblended lines (10%–20%); saturated lines are preceded by the symbol " > " and represent lower limits.

[b] Some contamination of C II] may be present from [O III] at 2320.9 Å.

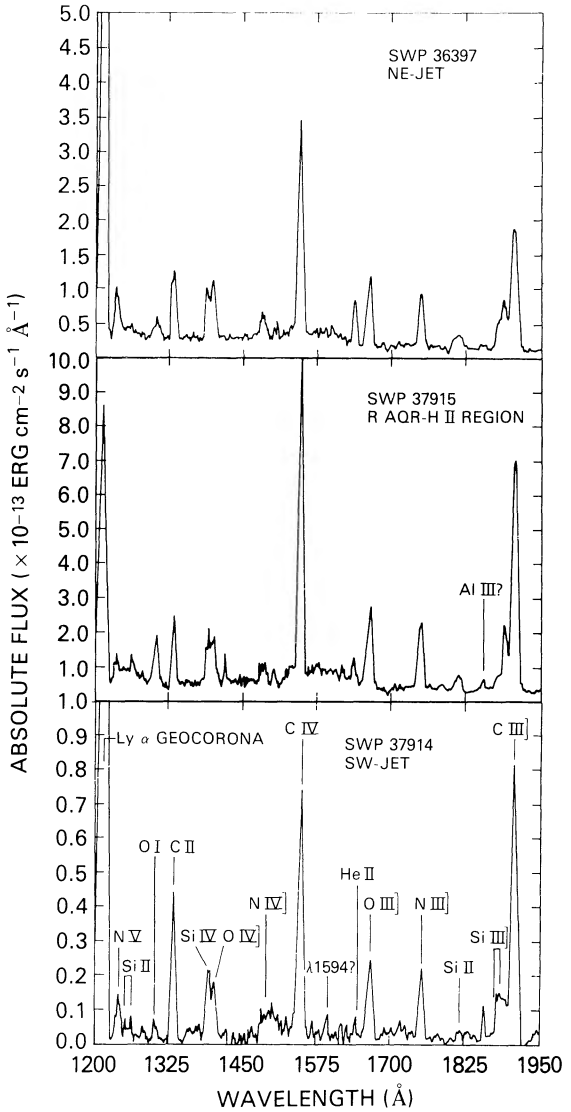

FIG. 1.—SWP 1200–2000 Å spectra of R Aqr for the NE jet (*upper panel*), the central H II region (*middle panel*), and the SW jet (*lower panel*). In both the NE and SW jet components the continuum is very weak relative to the central H II region, but high-excitation lines of N V at 1238 and 1242 Å and He II at 1640 Å are present. Si III] at 1892 Å in the jet components is weak compared with the H II region.

tent with the morphology in high-resolution radio maps of the NE jet features A and B (Kafatos et al. 1986). On the other hand, the *IUE* spectra of the weaker SW jet suggest that the emitting region may be more uniform, lacking distinct knots of emission in either radio continuum (Kafatos et al. 1989) or [O III] images (Hollis et al. 1990). We point out, however, that most of the jet emission is oriented along the dispersion direction of the *IUE* spectrometer. Thus, spatial inference from *IUE* data is considerably less than that possible from the aforementioned optical and radio data.

2.2. *Optical*

Long-slit optical spectrophotometry of R Aqr and the inner jet structure was obtained on 1989 November 19 and December 18 at the Lowell Observatory using the Ohio State University TI 800 × 800 CCD spectrograph attached to the Perkins 1.8 m reflector of the Ohio Wesleyan and Ohio State Universities. These observations utilized a 150 line mm^{-1} grating with a 2″ wide, 240″ long entrance slit aligned along the jet at a position angle of 29°, giving a spectral resolution of about 10 Å. The November and December observations covered the spectral regions 3400–7100 Å and 6000–9800 Å, respectively. Each observing session required two grating tilts with overlap regions containing Hβ or [O III] or Hα, as appropriate, to cover the given range. The spatial scale perpendicular to the dispersion direction was 0.″75 $pixel^{-1}$. An occulting wedge was used to block the light of the Mira to aid in observing the weaker NE and SW jets. To be able to define the spectrum extraction path, a short integration of R Aqr was also obtained without the wedge. Bias frames, flat-field spectra, Fe-Ne comparison spectra, and spectra of the standard star Feige 110 were obtained to provide wavelength and flux calibration.

Bias subtraction and flat-field correction were performed in IRAF using standard routines. After these steps, the long-slit spectra at a given grating tilt were averaged using median filtering to remove cosmic-ray events. The total integration times at the following grating tilt centers were achieved: 4550 Å (1500 s), 6000 Å (600 s), 7300 Å (1100 s), and 8700 Å (1100 s). Sky subtraction was effected by linearly interpolating between regions on the outside of the NE and SW jets.

Proper spectrum extraction for R Aqr and the NE and SW jets was complicated by atmospheric refraction. The blue spectrum (center at 4550 Å) was slightly curved by atmospheric refraction, while the red-sensitive TV camera introduced misalignment errors when centering the Mira on the slit. This caused a portion of the extreme blue end of the SW jet spectrum to be lost because of the overlap of the occulting wedge. The extraction path and width were chosen to include the complete spectrum from 3400 to 9800 Å of both jets. The NE jet spectrum was extracted from a 14″ long region centered at 13.″2 from R Aqr along the 29° position angle. The SW jet spectrum was extracted from a 14″ region centered at 12.″7 from R Aqr along a 209° position angle.

Although the occulting wedge eliminated most of the Mira light, the jet spectra still were contaminated by some scattered stellar light. To first-order correct the reduced jet spectra for scattered light, the spectrum of R Aqr was normalized at spectrum locations free from jet emission lines and then subtracted from the jet spectra. The spectra of the NE and SW jets are shown in Figure 2. Emission-line intensities were then extracted from the spectra and are summarized in Table 3.

2.3. *Comparison of Ultraviolet and Optical Line Fluxes*

In order to compare ultraviolet line fluxes in Table 2 to optical line fluxes in Table 3, we choose to scale the ultraviolet fluxes to the optical. Comparison between the *IUE* and optical spectroscopic data is complicated by at least two potential problems: (1) the different aperture sizes used by the two instruments and (2) extinction. In fact, Table 3 Hα/Hβ and Hγ/Hβ ratios and their estimated errors indicate very little extinction, since they are consistent with case B recombination values of 2.85 and 0.47, respectively, for an electron temperature $T_e \sim 10^4$ K and an electron density $n_e \sim 10^4$ cm^{-3}. There are indications that extinction toward the NE jet has been decreasing with time and is now negligible (Burgarella & Paresce 1991). Moreover, the *IUE* large aperture encompasses nearly all of the NE and SW emissions in their respective observations, while the 2″ wide slit for the optical data only samples the regions near the peaks of the jet emission; this aspect of any ultraviolet-optical comparison of our data is undoubtedly the largest single source of error. In any case, we simply assumed that the jet's [O III] 5007 Å emission (Hollis et al. 1990) is representative of the ultraviolet emission distribution, and appropriately superposed the 10″ × 20″ *IUE* aperture on both objects in this optical image as delineated in § 2.1 above. Similarly, we superposed the 2″ × 14″ aperture of the optical spectrometer as delineated in § 2.2 above and calculated the total fluxes. The resultant multipliers required to convert ultraviolet fluxes in Table 2 to the same scale as shown in Table 3 are 0.308 and 0.323 for the NE and SW jets, respectively. It is to be hoped that these factors provide a measure of the bulk properties of the peak emission regions in the different wavelength apertures, and, in fact, they seem to provide wavelength continuity when evaluating predicted line intensities derived from shock models discussed in the next section.

3. DISCUSSION

Now that symmetrical jet action in the R Aqr system has been unambiguously shown (Hollis et al. 1990), two key questions remain regarding the jet itself: (1) What is the nature of the jet excitation? (2) Is the jet causally related to the systemic inner nebulosity which is elongated north-south? Both of these questions were posed by Solf & Ulrich (1985) before the existence of the SW jet component had been established. Although no excitation modeling was offered, Solf & Ulrich suggested that the NE jet component could be excited by both ionizing ultraviolet radiation and shocks, citing line anomalies such as [O I] in the presence of [O III] as evidence for the presence of shock heating. With regard to the causal relationship between the NE jet and the inner nebulosity, Solf & Ulrich developed a detailed kinematical model of the inner nebulosity, from which they concluded that the jet knots and the inner nebulosity originated with the same explosive event ~180 yr earlier. The kinematical model was based on extensive long-slit spectrograms whose classic loop structures show that the inner nebulosity is an expanding shell, and the velocity field shows antisymmetry between the north and south shell halves. The spectrograms are essential to the morphological interpretation because the inner nebula is difficult to observe spatially because of its proximity to the light-dominant Mira which produces scattered or diffracted emission artifacts that can easily be confused with the inner nebulosity. Moreover, if the telescope secondary mirror supports lie at position angles near 45° and 135°, this further complicates the analysis.

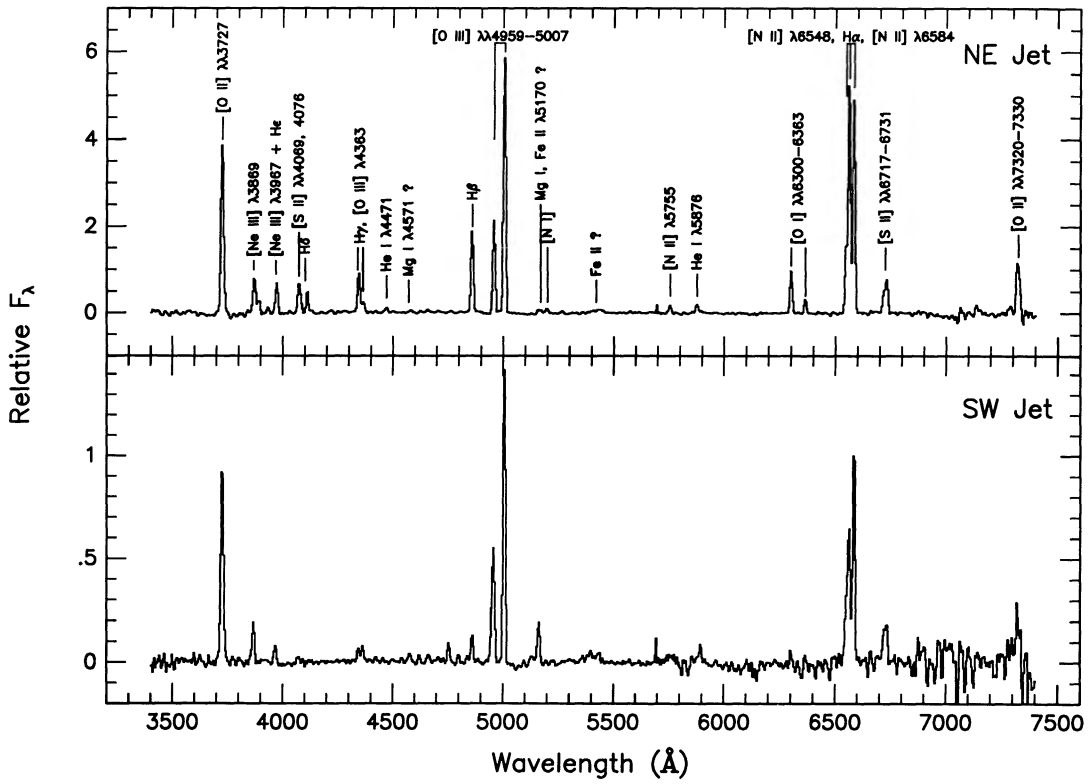

FIG. 2.—Low-resolution 3400–7400 Å spectra of the NE (*upper*) and SW (*lower*) jets in R Aqr. The principal emission features are indicated. The spectra longward of 7400 Å were not included, since the only detectable lines were [S III] at 9069 and 9531 Å.

TABLE 3

OPTICAL EMISSION-LINE FLUX MEASUREMENTS

Species	NE Jet (10^{-13} ergs cm^{-2} s^{-1})	NE Jet $F/F(H\beta)$	SW Jet (10^{-13} ergs cm^{-2} s^{-1})	SW Jet $F/F(H\beta)$
[O II] λλ3727, 3729	6.05	2.31	1.78	10.11
[Ne III] λ3869	1.31	0.50	0.34	1.91
Mg I?, [Fe II]? λ3832	0.24	0.09	<0.05	<0.28
Hε + He I λ3888	0.51	0.19	<0.05	<0.28
[Ne III] λ3967	0.92	0.35	0.14	0.77
[S II] λλ4069, 4076	1.15	0.44	0.06	0.33
Hδ λ4102	0.56	0.21	<0.05	<0.28
Hγ λ4340	1.35	0.52	0.10	0.56
[O III] λ4363	0.37	0.14	0.12	0.67
He I λ4471	0.21	0.08	<0.05	<0.28
Mg I λ4571?	0.10	0.04	<0.05	<0.28
Hβ λ4861	2.62	1.00	0.176	1.00
[O III] λ4959	2.85	1.09	0.79	4.50
[O III] λ5007	8.09	3.09	1.89	10.74
Mg I?, Fe II? λ5170	0.28	0.10	0.33	1.88
[N I] λ5200	0.23	0.09	<0.05	<0.28
[N II] λ5755	0.25	0.09	0.13:	0.74:
He I λ5876	0.32	0.12	0.14	0.80
[O I] λ6300	1.22	0.47	0.09	0.51
[O I] λ6363	0.40	0.15	<0.05	<0.28
[N II] λ6548	2.00	0.76	0.22	1.27
Hα λ6563	7.00	2.67	0.49	2.77
[N II] λ6584	6.30	2.41	0.74	4.18
[S II] λ6716	0.64	0.25	0.13	0.73
[S II] λ6731	1.08	0.41	0.11	0.63
[O II] λλ7320, 7330	2.28	0.87	<0.05	<0.28
[S III] λ9069	1.24	0.47	<0.05	<0.28
[S III] λ9531	2.29	0.87	<0.05	<0.28

NOTE.—1 σ errors: Lines stronger than Hβ (10%), weaker than Hβ (20%–50%), [O II] SW jet ~30%.

It is useful first to explore various ion line emission ratios from the jet optical spectra in order to test photoionization models in the low-density limit. As mentioned in § 2.3, Table 3 Hα/Hβ and Hγ/Hβ ratios indicate very little extinction, and we therefore adopt $E(B-V) = 0$ for this analysis. The usual diagnostic ratios are defined as

$$R([\text{O III}]) = (5007 + 4959)/4363 ,$$

$$R([\text{N II}]) = (6548 + 6583)/5755 ,$$

$$R([\text{S II}]) = 6716/6731 .$$

From Table 3, $R([\text{O III}]) \sim 29.6$ and $R([\text{S II}]) \sim 0.6$ yield $T_e \sim$ 26,000 K and $n_e \sim 4 \times 10^3$ cm^{-3} for the NE jet; similarly, $R([\text{O III}]) \sim 22.3$ and $R([\text{S II}]) \sim 1.2$ yield $T_e \sim 33{,}000$ K and $n_e \sim 4 \times 10^2$ cm^{-3} for the SW jet. It should be noted that our Table 3 [S II] λλ6716, 6731 intensities were the result of a two-component Gaussian model fit because they are blended as shown in Figure 2. By contrast, $R([\text{N II}]) \sim 33.2$ provides $T_e \sim 16{,}000$ K and $n_e \sim 3 \times 10^3$ cm^{-3} for the NE jet, and $R([\text{N II}]) > 9.6$ corresponds to upper limits of $T_e < 100{,}000$ K and $n_e < 6 \times 10^2$ cm^{-3} for the SW jet. Note that there is a weak T_e dependence in the $R([\text{S II}])$ density determination. In the NE jet, these different diagnostics suggest that the [O III] and [N II] emitting regions are probably not cospatial, since the ionization potentials are ~55 and ~30 eV, respectively, for these species. This situation is consistent with a shocked medium, which could explain the disparate temperatures.

3.1. *Shock Excitation*

Radiative shocks have the following observational characteristics at optical wavelengths (e.g., Shull & Draine 1987): (1) strong emission lines from underionized species such as [O I] λ6300, [N I] λ5200, [O II] λλ3727, 3729, and [S II] λλ6716, 6731 relative to Hβ; (2) a high electron temperature ($T_e > 2 \times 10^4$ K) measured by $R([\text{O III}])$; (3) the presence of a range of ionization states (e.g., [O I], [O II], and [O III]); and (4) large ratios of [O I] and [O II] relative to Hβ when compared with photoionized H II regions. The optical characteristics for both the NE and SW jets shown in Table 3 meet these criteria. We applied the MAPPINGS steady-flow shock code (Binette, Dopita, & Tuohy 1985) under a variety of physical conditions, but no single model could reproduce the observed [O II] and [O III] line ratios (see Table 3). Such modeling problems have been noted before in other clearly shocked objects (e.g., in the case of the Cygnus Loop filaments where [O I], [O II], and [O III] emission were seen to be noncospatial; see Fesen, Blair, & Kirshner 1982). While a combination of spectra from several models with a range of shock speeds (i.e., 80–130 km s^{-1}) could, in principle, reproduce the observations, there is clearly a vast amount of parameter space to explore based solely on the data in Tables 2 and 3. More likely, however, the emission variations seen in the observations of the NE and SW jets are due to the shock fronts encountering an inhomogeneous medium (cf. Fesen et al. 1982) which could produce a non–steady-flow shock (cf. Innes, Giddings, & Falle 1987). In any case, single steady-flow models generated for the spectrum of the NE jet with MAPPINGS were most successful in the case constrained to thermal equilibrium at a preshock temperature of 10,000 K with a preshock density of 200 cm^{-3}, which is representative of the temperature and density of the inner nebula and denser regions of the outer nebula (Hollis, Oliversen, & Wagner 1989).

The resultant model yielded a postshock transition zone $T_e \sim 1.2 \times 10^5$ K corresponding to a shock velocity of ~90 km s^{-1} which is comparable to the inner nebular expansion velocity at the position of the NE jet (Solf & Ulrich 1985). We were unable to achieve satisfactory results with a shock model in which no preionization was assumed, contrary to that adopted for the NE jet by Burgarella & Paresce (1991); our results require thermal equilibrium in a preshock region that has a T_e characteristic of that observed in the inner nebula. This could arise if ejecta forming the symmetrical jet impact the expanding shell of the inner nebula. This situation would argue that the R Aqr jet is younger than the ~180 yr old bipolar inner nebula.

The shock models also indicate that a modified solar abundance improves the synthetic NE jet spectrum in agreement with the ultraviolet and optical data. Specifically, nitrogen and oxygen were enhanced by factors of 2 and 1.5, while sulfur was reduced by a factor of ~3. The resultant abundance ratios C/N ~ 2.41 and O/N ~ 5.95 roughly agree with those independently derived by Nussbaumer et al. (1988) from ultraviolet observations of the R Aqr NE jet. These ratios compare favorably to similar values representative of M giants with little CNO-cycle processing (e.g., Nussbaumer et al. 1988).

The differences between the NE and SW jets are evident in the optical (Fig. 2 and Table 3). In particular, the higher [O III]/Hβ and lower [O II]/Hβ ratios in the SW jet suggest that the SW jet has a higher shock temperature. Models constructed for the SW jet crudely reproduced the observed spectrum when large changes in heavy-element abundances were introduced. However, one would expect that the NE and SW jets would have identical abundances. More likely, however, differences in preshock density, magnetic field, and shock velocity would produce an erroneous abundance anomaly (e.g., Shull & Draine 1987). Moreover, the SW jet may require a time-dependent model, since the SW jet seems to have developed only recently in the R Aqr system (Hollis et al. 1990). If the SW jet has just recently run into the inner nebulosity, then there may not have been sufficient time to develop a cooling recombination zone behind the shock. This seems very likely, since the recombination time scale for the gas is $\sim 3 \times 10^5$ yr/n_e (Dopita 1978) which is more than 100 yr for the densities inferred here. Cooling recombination zones can also be "truncated" by ionizing radiation, so that the low-ionization species do not have a chance to form. Hence, we are probably seeing both shocked jets evolving in spectral characteristics. Our shock models for both the SW and NE jets yield an n_e range ~10^3–10^4 cm^{-3}, which agrees with our ultraviolet observations as described in § 2.1.

In shock excitation, the higher ionization stages would be formed farther from the object, since ionization drops off behind the shock. However, the shock models that we have explored here predict average distances for the various coolant ions that cannot be spatially discriminated at the 250 pc distance of R Aqr. On the other hand, one would expect that thermal bremsstrahlung (free-free) radiation in the radio region would increase in emissivity as the gas is compressed behind the shock front. Moreover, as the gas temperature drops, the emissivity of the gas would increase, since the emission measure is proportional to the electron density and the inverse of the square root of the temperature. To investigate this effect, we have spatially compared emission features in the raw [O III] λ5007 image of R Aqr obtained with the *Hubble Space Telescope* (*HST*) faint object camera (FOC) at f/96 with our

previous 6 cm data contained in Kafatos et al. (1989) for optically thin and thermal radio jet features. (The R Aqr FOC image with file name x0c90101t was made available by the Space Telescope Science Institute as part of the Science Assessment and Early Release observations.) We find that these radio features are always closer to the central object than the corresponding [O III] line emission feature; the differences in positions range from $\sim 1''$ to $\sim 3''$, which correspond to 3.7×10^{15} to 1.1×10^{16} cm, respectively. This seems consistent with shock excitation in the R Aqr jet but may not be sufficient to eliminate other cases of photoionization discussed below.

3.2. *Photoionization Excitation*

Although we have shown that heating of jet knots is possible by shocks, photoionization of material may still be an important excitation mechanism. The flux distribution of continuum in the *IUE* wavelength range is difficult to determine because of the low signal-to-noise flux level of the continuum observed throughout the 1200–3200 Å range (see Fig. 1; also Kafatos et al. 1986). Determining the ultraviolet flux distribution is essential in order to assess the contribution of photoionization to heating. For example, the ultraviolet continuum associated with nova shells, such as Nova Her 1934 as observed with *IUE*, follows an empirical $L_\nu \propto \nu^{-2}$ luminosity distribution (Osterbrock 1989). In this case, O I is expected to be ionized to the $2p^3\,{}^2D$ level, which would be the main excitation of [O II] 3727 Å emission, rather than collisions (Osterbrock 1989). The formation of O^+ follows as a consequence of a large flux of photon energies above 13.6 eV, as expected from a ν^{-2} energy distribution. Thus, the large [O II] to [O III] ratio observed in the R Aqr symmetric jet could reflect a nonthermal photon flux distribution associated with a particular power-law spectrum. Moreover, there is a discrepancy (Osterbrock 1989) between observed and theoretical models for accretion disks in symbiotic systems and classical novae that renders this type of photoionization a possibility.

We derived the ionic abundances, extinction, and elemental abundances as described in Kafatos et al. (1986), where these parameters can be derived from the relative strengths of the assumed collisionally excited emission line in order to compare the results with time-dependent radiative cooling models in which a gas is suddenly photoionized and then cools faster than it recombines. In this analysis $E(B-V) = 0$ resulted in an underabundance of all heavy elements compared with their cosmic values (cf. Cameron 1973) when applied to the NE jet. A moderate extinction [i.e., $E(B-V) = 0.1$] afforded elemental abundances near or slightly above cosmic values for the NE jet. However, for the SW jet the assumption of no extinction resulted in appreciable overabundances compared with cosmic values.

In our abundance analysis that follows, we adopt the following conditions for the NE jet: $n_e \sim 4 \times 10^3$ cm^{-3}, $T_e \sim 26{,}000$ K, $E(B-V) \sim 0.1$, and the path length L through the emitting region is of order 10^{16} cm. We note that Kafatos et al. (1986) obtained $n_e \sim 10^4$ cm^{-3} for $T_e \sim 20{,}000$ K from their earlier data, which indicate that the NE jet excitation is increasing with time; we computed ionic and chemical abundances for these parameters as well, finding that the heavy-element abundances for this latter case were lower by a factor of 3, which would require a higher extinction in the NE jet. Similarly, for the SW jet we adopt $n_e \sim 4 \times 10^2$ cm^{-3}, $T_e \sim 33{,}000$ K, $E(B-V) \sim 0$, and $L \sim 10^{16}$ cm.

The results for the NE and SW jets are shown in Table 4. We expect other ions which do not have emission lines in the ultraviolet or optical ranges that we observed to also be present, such as N VI, O VII, O VI, O V, and Si V and have so indicated in Table 4 by a question mark. The results for carbon in the NE jet are suspect because they depend solely on the ionic abundance N(C II) estimated from the C II] line in the long-wavelength region of the *IUE* spectrum, which has some contamination from [O III] (see Table 2). Both N(C II) and the abundance of carbon relative to the cosmic value are, therefore, upper limits. Since we do not have a long-wavelength range *IUE* spectrum for the SW jet, our estimate of the N(C II) and the corresponding chemical abundance of carbon is a lower limit.

In this particular analysis, carbon, oxygen, and nitrogen are overabundant in both jets, while silicon is underabundant and probably locked up in grains (Kafatos et al. 1986). Since the silicon abundance is slightly below or near its cosmic value, it argues in a self-consistent way that the reddening is small in the SW jet. A higher extinction in the NE jet would bring the abundances of the two jets closer to each other, although the result would cause higher ionization stages to be excited (e.g., N V). Moderate to low values of extinction (e.g., $E(B-V) \sim 0.1$] have been assumed in all previous work, and the present work does not require higher values.

The ionic abundances of Table 4 can be compared with

TABLE 4

IONIC AND CHEMICAL ABUNDANCES IN THE R AQUARII JET

Species	NE Jet[a]	SW Jet[b]
Ionic Abundances		
N VI	?[c]	?[c]
N V	0.1199	0.0396
N IV	0.0744	0.0443
N III	0.5695	0.5520
N II	0.1866	0.3640
N I	0.0496	?[d]
O VII, VI, V	?[c]	?[c]
O IV	0.0790	0.0747
O III	0.3375	0.6324
O II	0.2649	0.1093
O I	0.3186	0.1837
C V	?[c]	?[c]
C IV	0.0453	<0.2698[e]
C III	>0.1490[f]	<0.7372[e]
C II	<0.8057[g]	?[e]
Si V	?[c]	?[c]
Si IV	0.2098	0.5829
Si III	0.6608	0.2369
Si II	<0.1294[h]	0.1802
Chemical Abundances/Cosmic Abundances		
N	1.45	4.09
O	1.71	4.25
C	<5.0[g]	>1.53[e]
Si	0.26	0.71

[a] $n_e \sim 4 \times 10^3$ cm^{-3}, $T_e \sim 26{,}000$ K, and $E(B-V) \sim 0.1$.
[b] $n_e \sim 4 \times 10^2$ cm^{-3}, $T_e \sim 33{,}000$ K, and $E(B-V) \sim 0$.
[c] These ions should be present if cooling is time-dependent and temperatures are in the range 10^4–10^5 K.
[d] [N I] not observed in SW jet.
[e] C II] should be present, but no spectrum was taken.
[f] C III] saturated.
[g] May be overestimated because of [O III] contamination of the C II] line.
[h] Si II not observed in SW jet.

time-dependent radiative cooling models of Kafatos (1973) and Shapiro & Moore (1976) in which a gas is not in ionization equilibrium. The present data favor this mechanism from two standpoints: (1) the lower density SW jet is hotter than the denser NE jet, and (2) a wide variety of ionic stages are seen in both jets.

To estimate the cooling time scales for both jets, we assume that the initial temperature of the gas in both jets was $\sim 10^5$ K and is now 33,000 K for the SW jet and 26,000 K for the NE jet. These assumptions yield the following time scales (Kafatos 1973):

$$t_{SW} \sim 2660 \text{ yr}/(n_e \times R), \quad t_{NE} \sim 3960 \text{ yr}/(n_e \times R),$$

where R is the ratio of computed heavy-element abundance in Table 4 to the corresponding cosmic value. In the case of the SW jet, $R \sim 4.0$ and $n_e \sim 400$ cm^{-3} yields $t_{SW} \sim 1.7$ yr, while in the NE jet, $t_{NE} \sim 0.66$ yr, using $R \sim 1.5$ and $n_e \sim 4 \times 10^3$ cm^{-3}. As expected, the hotter, less dense SW jet cools more slowly than the more dense NE jet when excited to a higher temperature. Both jet cooling time scales are much shorter than most of the temporal variations reported previously in R Aqr and provide support to the suggestion that the jet features are photoexcited on time scales of $\sim$1–1.5 yr as a result of the instabilities in the inner accretion disk around the hot companion (Kafatos et al. 1986).

A wide variety of ionic stages are expected in time-dependent radiative cooling as compared with steady state collisional heating. However, comparing the results of Table 4 with models in Kafatos (1973) and Shapiro & Moore (1976) suggests that a single density and temperature for each jet is too simple. Density and temperature gradients could, in principle, produce agreement with the observations. In time-dependent cooling, the higher ionization stages would be found closer to the central object, since higher energy radiation would be absorbed nearer the photoionizing source. However, recent [O III] λ5007 and [O II] λ3727 images of the NE jet of R Aqr obtained with the *HST* FOC (STScI publicity photographs) show no positional differences for the features in these emission lines.

3.3. *Age of the Jets*

Kinematic arguments support the contention that the R Aqr jet was not formed at the same time as the inner nebula. From the spectroscopic data in Figure 6 of Solf & Ulrich (1985), an observed radial velocity gradient of ~ -1.90 km s^{-1} arcsec^{-1} along the NE jet can be deduced, although Solf & Ulrich themselves quote -1.40 km s^{-1} arcsec^{-1}; similarly, the inner nebular expansion model velocity gradient of -2.89 km s^{-1} arcsec^{-1} at the position of the NE jet can be obtained from Figure 9 of Solf & Ulrich (1985). Since the observed and modeled velocity gradients are different, it is difficult to conclude that the jet features are part of the expanding inner nebula model. Solf & Ulrich (1985) acknowledged this problem in their interpretation, but their earlier data did not reveal a SW countepart to the NE jet. They contended that the NE jet was really an isolated local condensation on the inner nebula that had vastly decelerated in the recent past following the formation of the inner nebula.

To be younger than the $\sim$180 yr old inner nebula, the NE and SW jet features must each have a space velocity in excess of the inner nebular expansion velocity ($\sim$90 km s^{-1} from the Solf & Ulrich model) at their projected positions on the surface of the inner nebula. With high-resolution spectroscopy, Hollis et al. (1990) have shown that such velocities are possible, and if the jet is tilted less than 20° to the plane of the sky, then a velocity differential between the NE and SW jet exceeds $\sim$300 km s^{-1}. This would correspond to a simple expansion age of less than 90 yr. There is evidence to support an $\sim$20° tilt to the jet axis: mass loss confined to the orbital plane appears to be radially symmetric as it leaves the system (Solf &Ulrich 1985); this would produce a circular outer nebula. However, the appearance of the outer nebula is ellipsoidal with an axial ratio of 1:3. This suggests that the axis of the orbital plane would be tilted out of the plane of the sky toward the observer by $\sim$20° (cf. Wallerstein & Greenstein 1980; Solf & Ulrich 1985). If the accretion disk, which presumably powers the symmetrical jet, is not precessing, then from angular momentum arguments the symmetrical jet axis arising from an accretion disk surrounding the hot companion would be parallel to the orbital axis. However, the accretion disk may be precessing (Michalitsianos et al. 1988; Kafatos et al. 1989).

In any case, Figure 3 suggests the orientation of the expanding inner nebula model with respect to a contour map of the NE and SW jets. Figure 3 schematically shows the expanding outer surface of the inner nebulosity model advocated by Solf & Ulrich (1985), and the symmetrical jet in [O III] 5007 Å emission (Hollis et al. 1990). From kinematic data Solf & Ulrich argue that the inner nebular expansion velocity (V_E) is

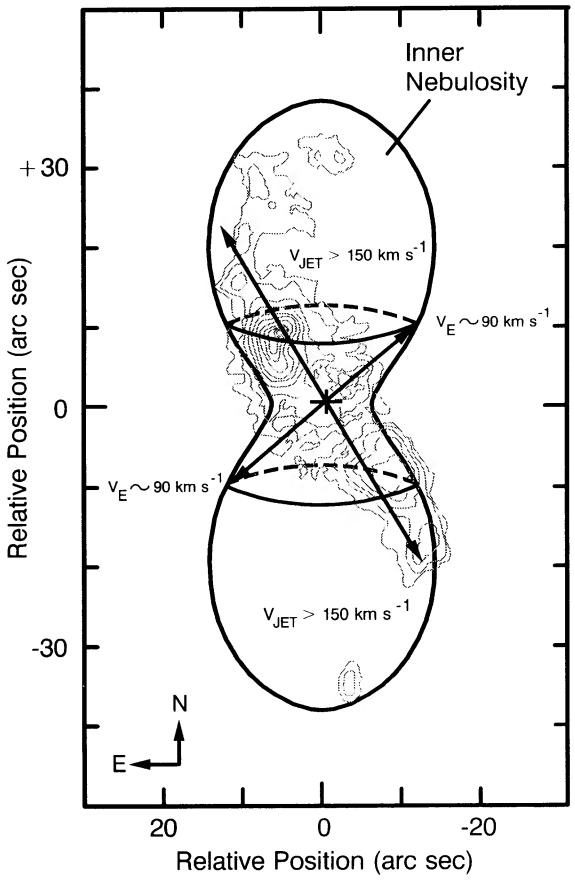

FIG. 3.—Shown schematically is the expanding outer surface of the inner nebulosity model of Solf & Ulrich (1985). Also shown embedded in the inner nebulosity model is the symmetrical jet in [O III] 5007 Å emission (Hollis et al. 1990). The jets may be brightening as they impact the expanding inner nebula (see text for discussion).

latitude- (ϕ-) dependent and can be represented by $V_E(\phi) = 32 + 168 \sin^4 |\phi|$. In projection we see the peak emission of the NE and SW jets located at about $\phi \sim 49°$ if they were on the surface of the expanding inner nebula; at this location $V_E \sim 90$ km s^{-1}. If the major axis of the inner nebula is perpendicular to the orbital plane of the binary system, then the NE-SW jet axis must be somewhat inclined to the orbital plane. In such an instance, one can make arguments for a precessing accretion disk (Michalitsianos et al. 1988). Hence, the jets may be brightening as they impact the expanding inner nebula. Unfortunately, the three-dimensional aspect of the NE-SW jet is not known and remains one of the most significant problems for solution in this intriguing binary system.

3.4. *Summary*

We have shown that the SW jet is detectable in the radio (Kafatos et al. 1989), optical (Hollis et al. 1990), and now the ultraviolet. Additionally, we argue for a younger age for the R Aqr symmetrical jet (<90 yr) as compared with the age of the inner nebulosity (~ 180 yr). Moreover, we have also shown the difficulty in determining whether the excitation of the jet is caused predominantly by shock heating or photoionization. While the NE and SW jets could be excited by a shock mechanism as the material of the jet impacts the inner edge of the expanding inner nebulosity, no simple steady-flow shock model for each jet component is sufficient. In all likelihood any shock front would encounter an inhomogeneous medium which could cause dynamical instabilities. The high [O III] temperatures for both the NE (26,000 K) and SW (33,000 K) jet components could be explained by the shock mechanism with preshock excitation in thermal equilibrium. However, the jet components are undoubtedly evolving with time, and therefore we have also considered the case of time-dependent radiative cooling after an initial photoionization of both jets; in this case, density and temperature gradients must be invoked to produce agreement with the observed line emission in the ultraviolet and optical wavelength ranges. Both the steady-flow shock model and time-dependent cooling models produce abundance differences in the two jets, which seems unlikely. Further, we note that photoionization by a power-law spectrum also may be possible, but the exact form of the spectrum for accretion disks in symbiotic systems is highly uncertain.

We thank M. Dopita and S. Meatheringham for providing the use of the shock modeling program to aid our analysis, and I. Evans for his helpful documentation of it. We are grateful to B. Draine, R. Goodrich, R. Fesen, and M. Shull for their useful comments.

REFERENCES

Binette, L., Dopita, M. A., & Tuohy, I. R. 1985, ApJ, 297, 476
Burgarella, D., & Paresce, F. 1991, ApJ, 370, 590
Cameron, A. G. 1973, Space Sci. Rev., 15, 121
Cassatella, A., Lioyd, C., & Gonzalez Riestra, R. 1988, ESA-IUE Newsletter, No. 31, p. 13
Dopita, M. A. 1978, ApJS, 37, 117
Fesen, R. A., Blair, W. P., & Kirshner, R. P. 1982, ApJ, 262, 171
Herbig, G. 1980, IAU Circ., No. 3535
Hollis, J. M., Kafatos, M., Michalitsianos, A. G., & McAlister, H. A. 1985, ApJ, 289, 765
Hollis, J. M., Oliversen, R. J., & Wagner, R. M. 1989, ApJ, 337, 795
Hollis, J. M., Wagner, R. J., & Oliversen, R. J. 1990, ApJ, 351, L17
Innes, D. E., Giddings, J. R., & Falle, S. A. E. G. 1987, MNRAS, 226, 67
Kafatos, M. 1973, ApJ, 182, 433
Kafatos, M., Hollis, J. M., & Michalitsianos, A. G. 1983, ApJ, 267, L103
Kafatos, M., Hollis, J. M., Yusef-Zadeh, F., Michalitsianos, A. G., & Elitzur, M. 1989, ApJ, 346, 991
Kafatos, M., Michalitsianos, A. G., & Hollis, J. M. 1986, ApJS, 62, 853
Mauron, N., Nieto, J. L., Picat, J. P., Lelievre, G., & Sol, H. 1985, A&A, 142, 413
Michalitsianos, A. G., & Kafatos, M. 1982, ApJ, 262, L47
Michalitsianos, A. G., Oliversen, R. J., Hollis, J. M., Kafatos, M., Crull, H. E., & Miller, R. J. 1988, AJ, 95, 1478
Nussbaumer, H. 1986, A&A, 155, 205
Nussbaumer, H., Schild, H., Schmid, H. M., & Vogel, M. 1988, A&A, 198, 179
Osterbrock, D. E. 1989, Astrophysics of Gaseous Nebulae and Active Galactic Nuclei (Mill Valley: University Science Books), chap. 10
Paresce, F., Burrows, C., & Horne, K. 1988, ApJ, 329, 318
Shapiro, P. R., & Moore, R. T. 1976, ApJ, 207, 460
Shull, J. M., & Draine, B. T. 1987, in Interstellar Processes, ed. D. J. Hollenbach & H. A. Thronson (Dordrecht: Reidel), 283
Solf, J., & Ulrich, H. 1985, A&A, 148, 274
Turnrose, B. E., & Thompson, R. W. 1984, *IUE* Image Processing Information Manual, Version 2.0 (CSC/TM-84/6058)
Wallerstein, G., & Greenstein, J. L. 1980, PASP, 92, 275
Whitelock, P. A. 1987, PASP, 99, 573